

# **Divergent evolution of protein conformational dynamics in dihydrofolate reductase**

Gira Bhabha, Damian C. Ekiert, Madeleine Jennewein, Christian M. Zmasek, Lisa M. Tuttle, Gerard Kroon, H. Jane Dyson, Adam Godzik, Ian A. Wilson and Peter E. Wright

## **Supplementary Information:**

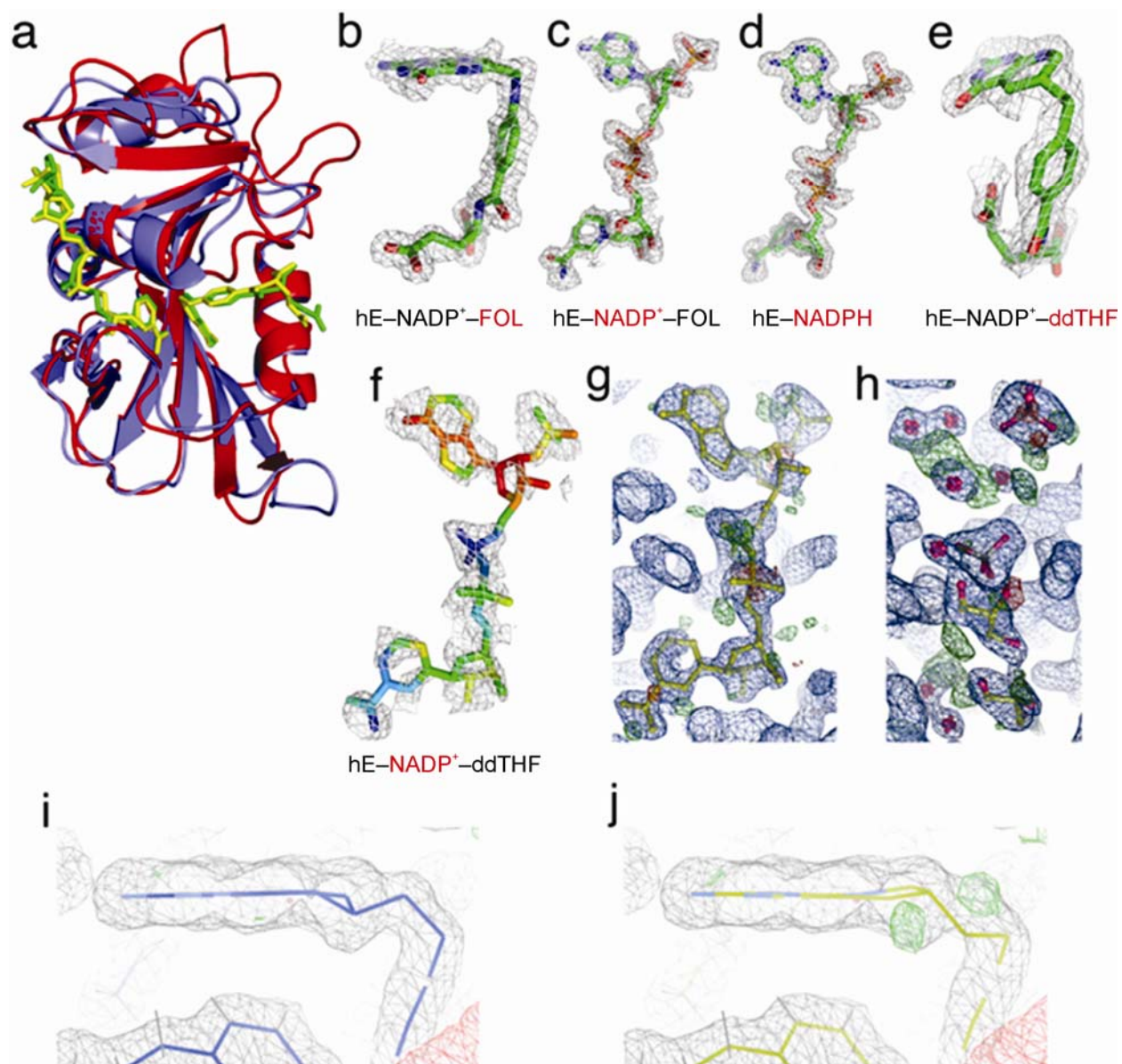
Supplementary Figures 1-6

Supplementary Tables 1-4

Supplementary Note

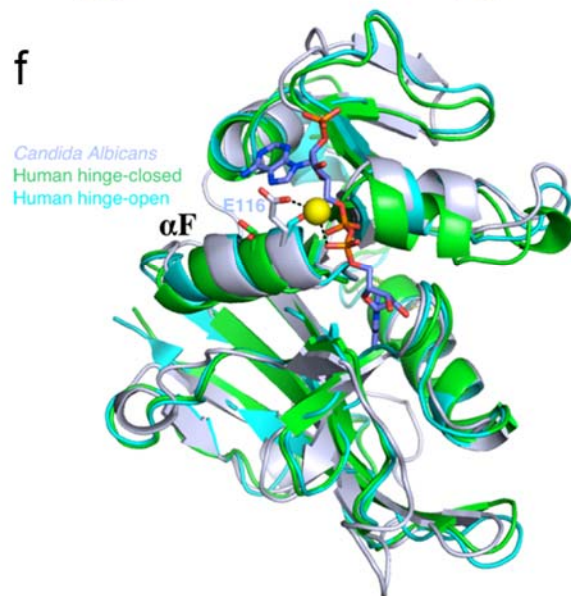
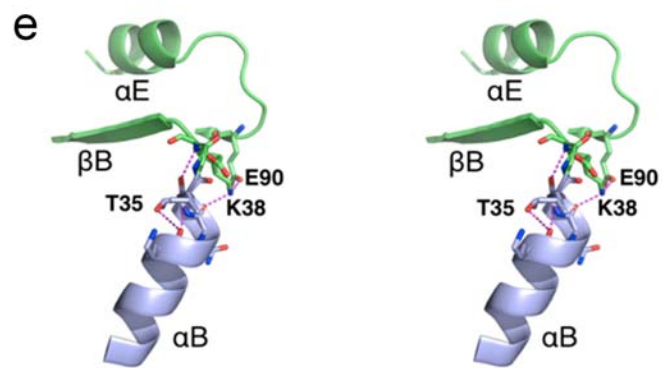
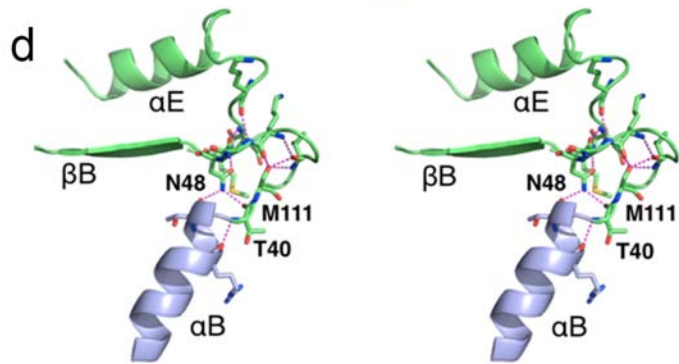
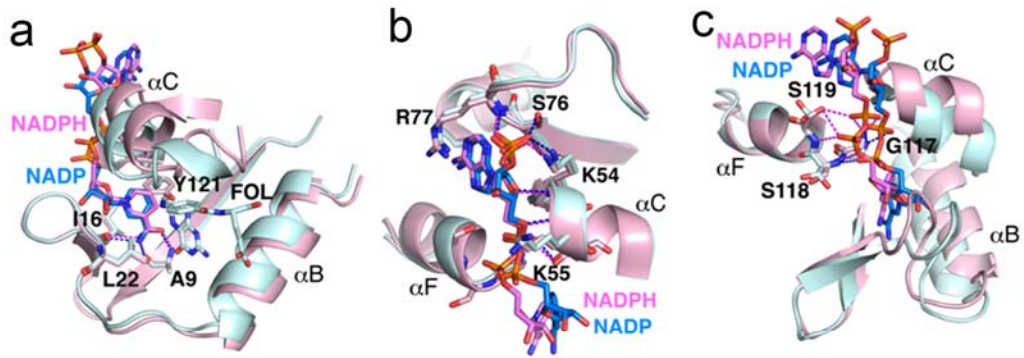
References

## Supplementary Figures

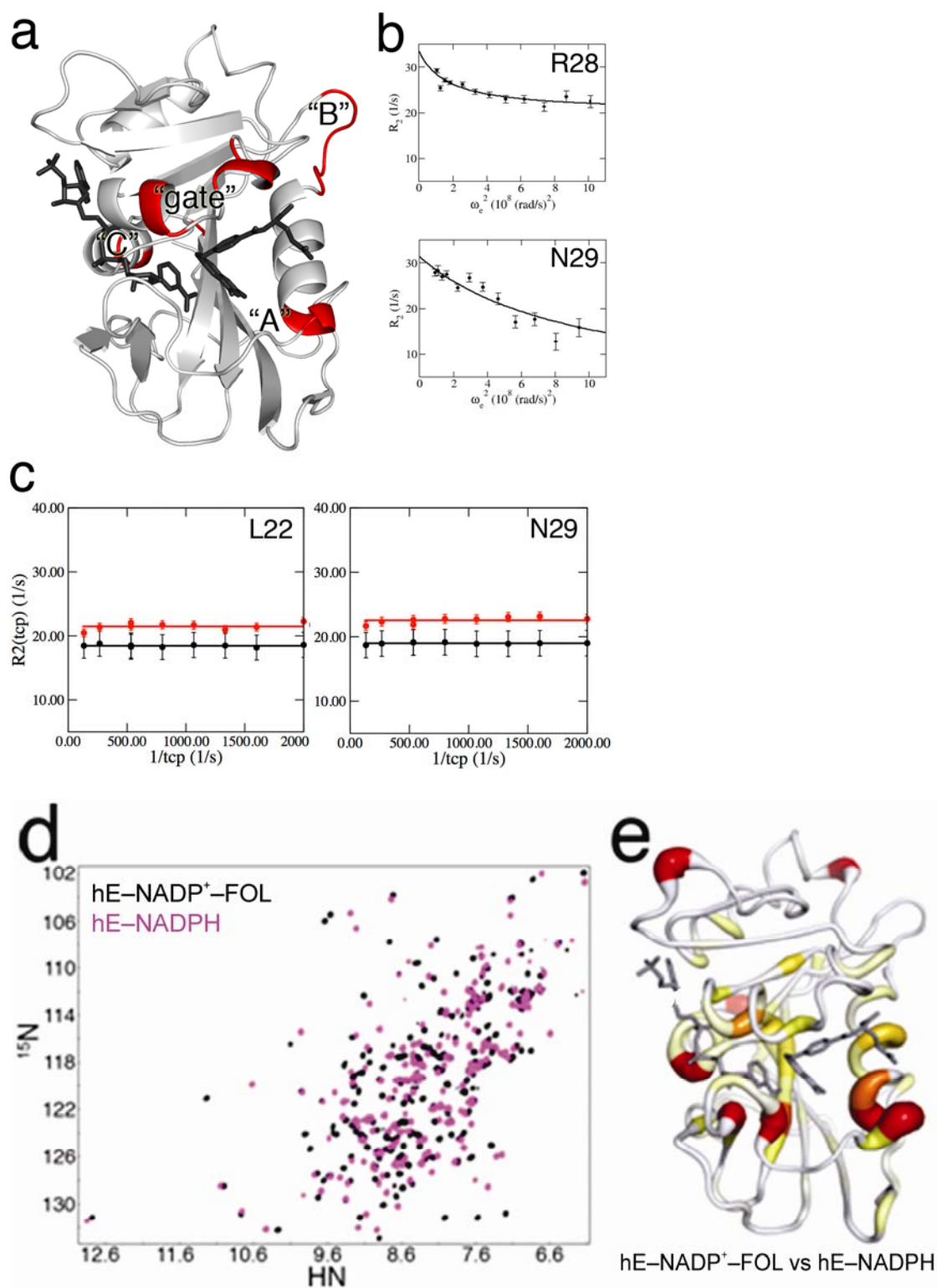


**Supplementary Figure 1. X-ray structures and omit maps for ligands built into hDHFR structures.** (a) Overlay of ecDHFR (PDB code 1RX2<sup>1</sup>) and hDHFR bound to NADP<sup>+</sup> and folate, showing that hDHFR and ecDHFR are highly conserved at the structural level. ecDHFR is shown in purple with green ligands, and hDHFR is shown in red with yellow ligands. (b-f) 2F<sub>O</sub>-F<sub>C</sub> omit maps are shown for each ligand, contoured to  $\sigma = 1.0$ . (b) Folate from the hE-NADP<sup>+</sup>-FOL structure. (c) NADP<sup>+</sup> from the hE-NADP<sup>+</sup>-FOL structure. (d) NADPH from the hE-NADPH structure. (e) ddTHF from the hE-NADP<sup>+</sup>-ddTHF structure. (f) NADP<sup>+</sup> from the hE-NADP<sup>+</sup>-ddTHF structure, the NADP<sup>+</sup> is colored by B-factor, after final refinement. (g-h) As discussed in the text, the density for this NADP<sup>+</sup> ligand was discontinuous, indicating disorder and/or low occupancy. (g) Ligand occupancy was refined using PHENIX, and the ligand is

modeled in at an occupancy of  $\sim 0.8$ .  $2F_O-F_C$  map ( $\sigma = 1$ ; blue) and  $F_O-F_C$  map ( $\sigma = 3$ ; red, negative density; green positive density) after refinement with  $\text{NADP}^+$  modeled into the hE– $\text{NADP}^+$ –ddTHF structure. **(h)**  $2F_O-F_C$  map ( $\sigma = 1$ ; blue) and  $F_O-F_C$  map ( $\sigma = 3$ ; red, negative density; green positive density) after refinement with 2 phosphates, 2 glycerols and waters modeled into the NADP-binding site in the hE– $\text{NADP}^+$ –ddTHF structure. Remaining positive density is observed in the adenine region and the nicotinamide region, showing that the density is not satisfied upon modeling in buffer molecules. **(i)**  $2F_O-F_C$  map ( $\sigma = 1$ ; grey) and  $F_O-F_C$  map ( $\sigma = 3$ ; red, negative density; green positive density) after refinement with 6S-ddTHF (blue sticks). **(j)**  $2F_O-F_C$  map ( $\sigma = 1$ ; grey) and  $F_O-F_C$  map ( $\sigma = 3$ ; red, negative density; green positive density) after refinement with 6R-ddTHF (yellow sticks).



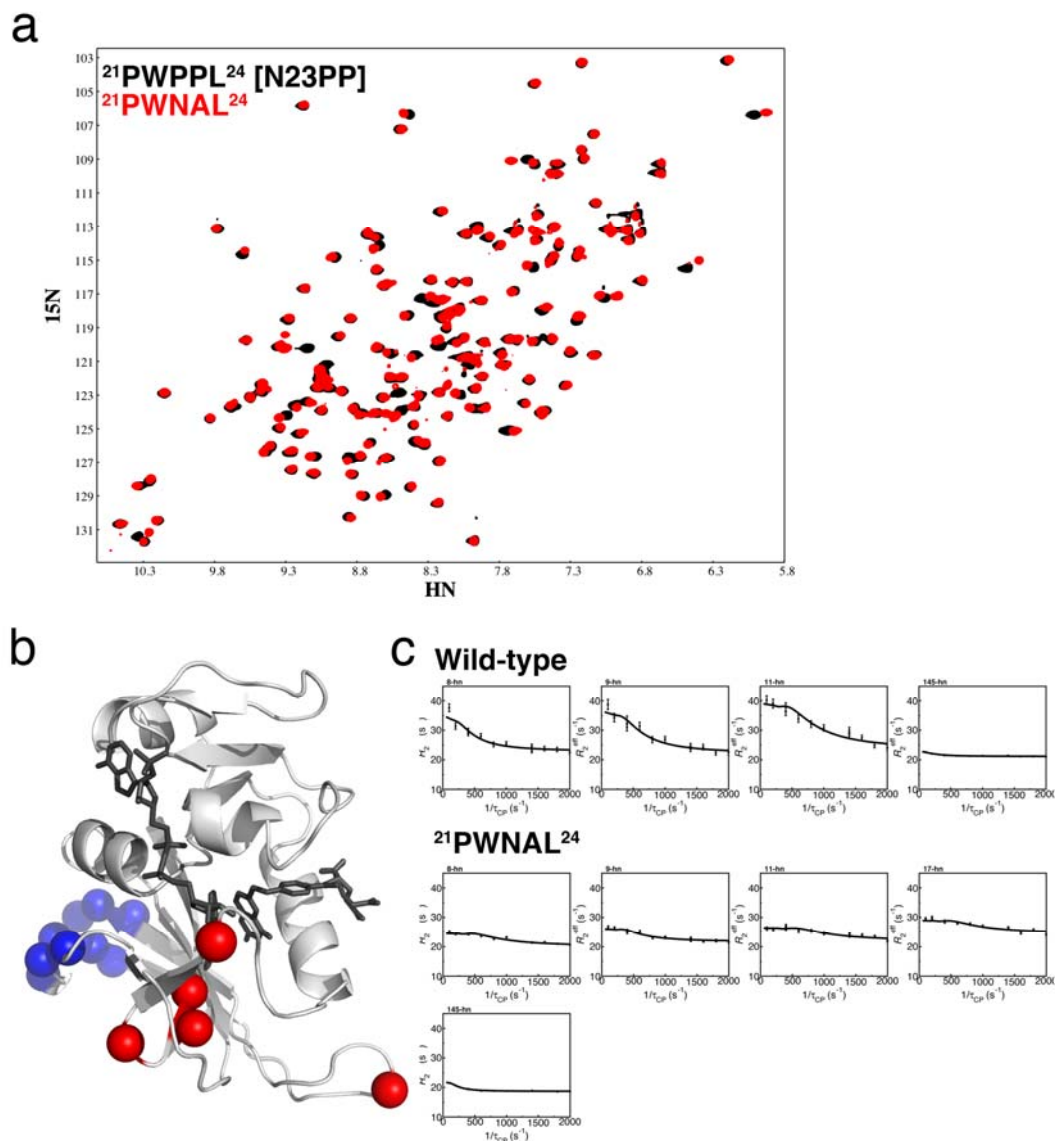
**Supplementary Figure 2. Hydrogen bonding networks that support the hinge-open conformation. (a-c)** Overlay of hE–NADP<sup>+</sup>–FOL (cyan) and hE–NADPH (light pink), aligned on the “Met20” loop **(a)**, residues 71-114 **(b)** and helix  $\alpha$ F **(c)**. NADP<sup>+</sup> corresponding to hE–NADP<sup>+</sup>–FOL is in blue, and NADPH corresponding to the hE–NADPH structure is in pink. Ligands and side chains are colored by element: nitrogen blue, oxygen red, phosphorus orange, carbon as described for each ligand or structure. Hydrogen bonds are shown as blue dashed lines for E–NADP<sup>+</sup>–FOL and pink dashed lines for E–NADPH. Hydrogen bonds stabilizing the nicotinamide moiety **(a)** and the adenosine moiety **(b)** are present in both conformations. **(c)** Hydrogen bonds from the diphosphate groups of NADPH to Ser119 (pink dashed lines) stabilize the “hinge-open” conformation. These hydrogen bonds are broken in the “hinge-closed” conformation, as other hydrogen bonds are formed to folate (Supplementary Table 2). **(d-e)** Hydrogen bonds for Hinge 1 in hDHFR **(d)** and ecDHFR **(e)**. Many hydrogen bonds stabilize Hinge 1 in human DHFR. Residues in the loop subdomain are colored purple, and residues in the adenosine-binding subdomain are coloured green. **(f). The hinge-open conformation is stabilized in *C. albicans* DHFR.** An overlay of caDHFR bound to NADPH (purple, PDB code: 1AI9<sup>2</sup>) with hE–NADP<sup>+</sup>–FOL (green, hinge-closed) and hE–NADPH (cyan, hinge-open) show that the  $\alpha$ F helix in cDHFR is aligned with that in hE–NADPH. The structures are aligned on the loop subdomain. Ser119, which stabilizes the hinge-open conformation in hDHFR, has been substituted with Glu116 in caDHFR, which can also stabilize the hinge-open conformation via a water-mediated hydrogen bond to NADPH.



**Supplementary Figure 3. Supporting NMR data for hDHFR.** (a-c) Numerous residues in hE-NADP<sup>+</sup>-FOL show <sup>15</sup>N R<sub>1ρ</sub> dispersion at 280 K, but <sup>15</sup>N R<sub>2</sub> dispersion is not observed in hDHFR. (a) Selected residues showing <sup>15</sup>N R<sub>1ρ</sub> dispersion in regions A, B and C as well as a

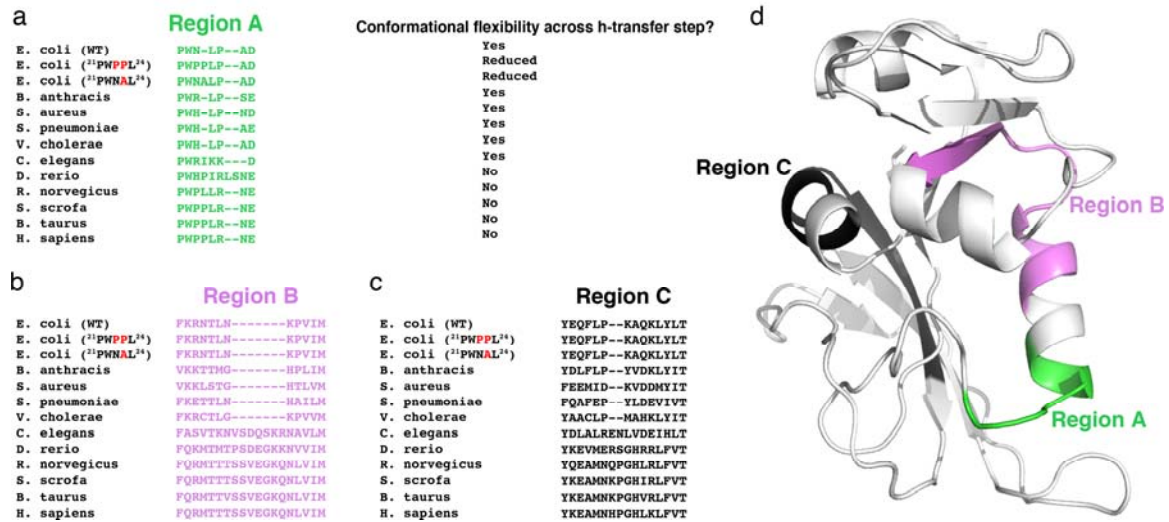
region that likely “gates” NADP flux are shown in red on the hE–NADP<sup>+</sup>–FOL structure. Ligands are shown as sticks. **(b)** Examples of R<sub>1ρ</sub> dispersion curves. Residue numbers are indicated in the top right for each curve. **(c)** Representative data for hE–NADP<sup>+</sup>–FOL <sup>15</sup>N R<sub>2</sub> dispersion experiments at 500 MHz (black) and 800 MHz (red). These data were collected at 303 K. No dispersion was observed for data collected at 280 K, 292K, 298 K, or 309 K. **(d-e)** <sup>15</sup>N <sup>1</sup>H chemical shift differences in hDHFR binary and ternary complexes. **(d)** Overlay of hE–NADP<sup>+</sup>–FOL (black) and hE–NADPH (magenta) <sup>15</sup>N HSQC spectra at pH 8.0 and a temperature of 300 K. **(e)** Weighted average <sup>1</sup>H, <sup>15</sup>N chemical shift differences between hE–NADP<sup>+</sup>–FOL and hE–NADPH (shown in A), mapped onto the hDHFR structure. Chemical shift differences are colored onto the structure using a gradient of thickness and red to white, with red, thick regions representing the largest chemical shift differences between the two complexes; ligands are shown as dark gray sticks. Large changes are observed in helix αF and hinge 2. Chemical shift differences were calculated as follows:

$$\sqrt{(\Delta^1\text{H})^2 + \left(\frac{\Delta^{15}\text{N}}{5}\right)^2}$$

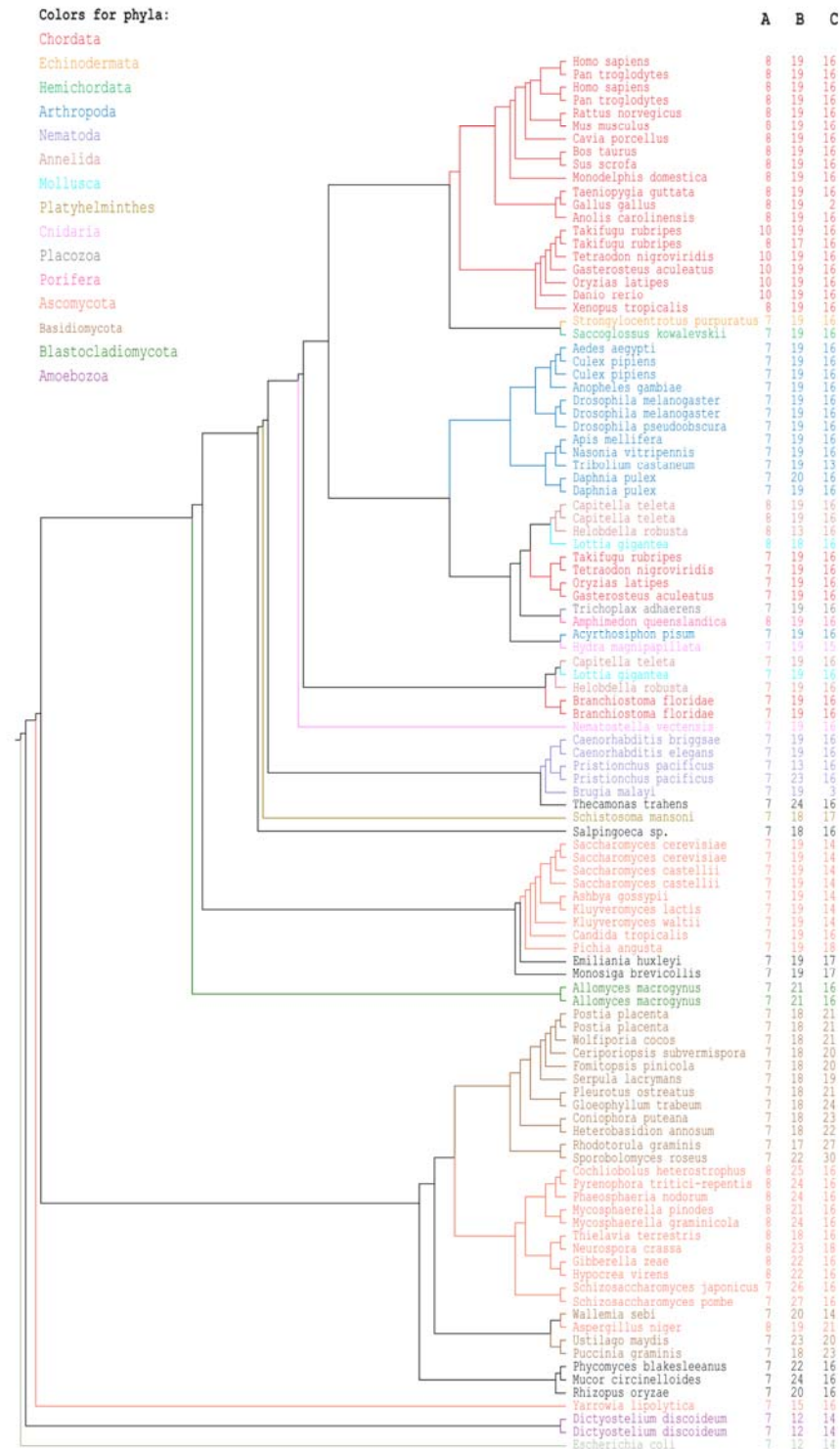


**Supplementary Figure 4. Supporting NMR data for  $^{21}\text{PWNAL}^{24}$  ecDHFR mutant.** (a) The  $^{21}\text{PWNAL}^{24}$  *E. coli* DHFR mutant is structurally similar to N23PP (or  $^{21}\text{PWPPL}^{24}$ ) ecDHFR. Overlay of  $^{21}\text{PWNAL}^{24}$  ecDHFR  $^{15}\text{N}$  HSQC spectrum (red) with N23PP ecDHFR  $^{15}\text{N}$  HSQC spectrum (black), with both enzymes bound to  $\text{NADP}^+$  and FOL, showing that resonances do not shift significantly. (b-c)  $^{15}\text{N}$   $R_2$  dispersion is present, but considerably dampened, for a few active site residues in  $^{21}\text{PWNAL}^{24}$  ecDHFR. (b) Residues showing  $^{15}\text{N}$   $R_2$  dispersion in relaxation compensated constant time CPMG experiments are plotted as spheres on the wild type ecDHFR– $\text{NADP}^+$ –FOL structure (3QL0<sup>3</sup>). Dispersion profiles for C-terminal associated residues (blue) are unaffected by the mutation. All other residues exhibiting dispersion are located in the active site and are shown in red. (c).  $^{15}\text{N}$   $R_2$  dispersion curves for active site residues in the mutant, and corresponding curves for the wild type enzyme. The few residues that do show dispersion in the mutant have significantly reduced  $R_{\text{ex}}$  values.

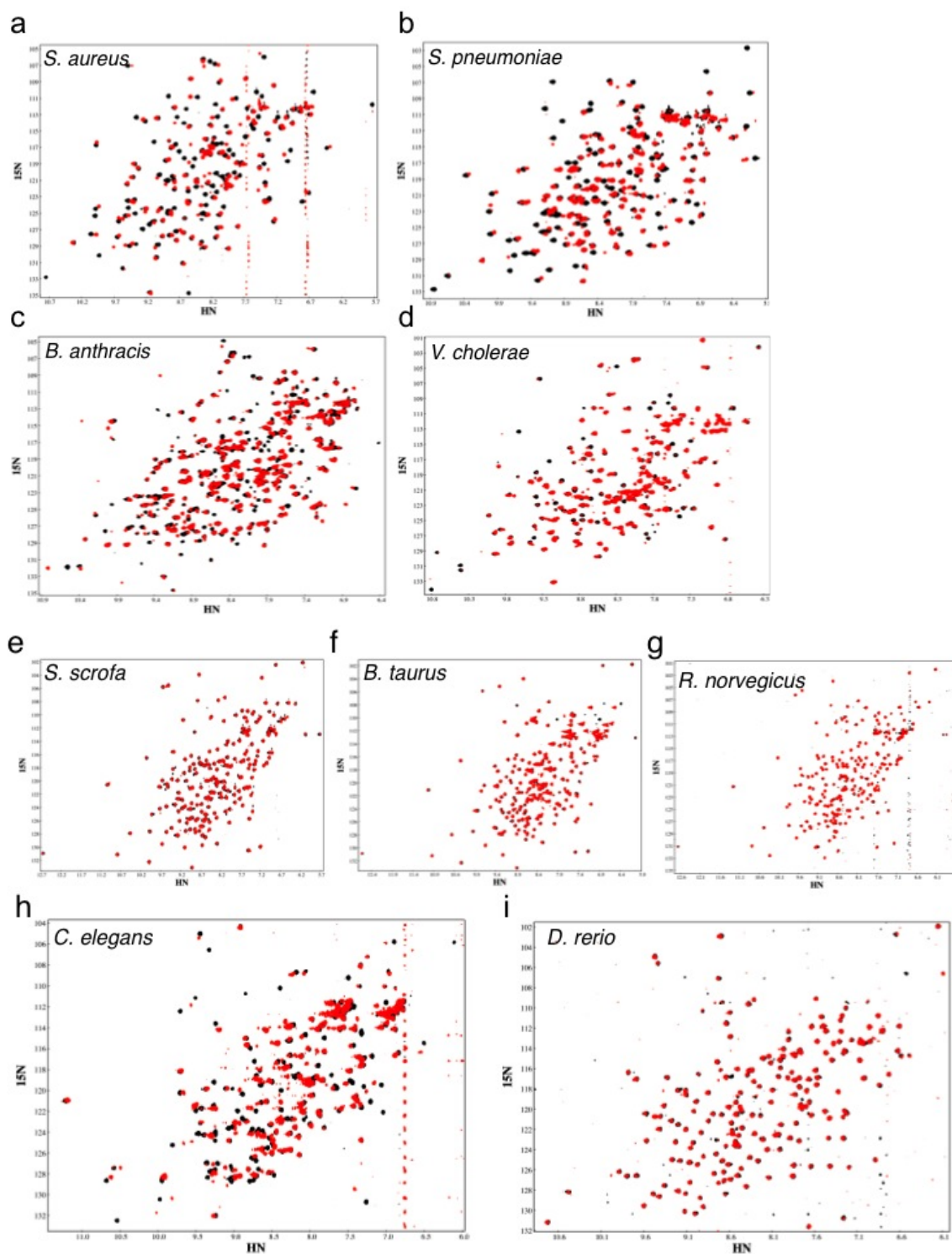




e



**Supplementary Figure 5. Sequence analysis of DHFRs from different species. (a-d)** Sequence alignments of DHFR enzymes for which NMR data were obtained. **(e)** Tree of eukaryotic DHFR sequences showing lengths of Regions A, B and C. *E. coli* DHFR is also shown for comparison.



**Supplementary Figure 6.**  $^{15}\text{N}$  HSQC spectra for bacterial DHFRs (a-d) and eukaryotic DHFRs (e-i). Spectra show DHFRs in the E-NADP<sup>+</sup>-FOL (black) or E-NADP<sup>+</sup>-THF (red) complexes. Spectra are shown for *S. aureus* (a), *S. pneumoniae* (b), *B. anthracis* (c), *V. cholerae* (d), *S. scrofa* (e), *B. taurus* (f), *R. norvegicus* (g), *C. elegans* (h), and *D. rerio* (i).

Supplementary Tables

Supplementary Table 1. Ligand-protein hydrogen bonds in hDHFR

hE–NADP <sup>+</sup> –FOL			hE–NADPH		
Donor	Acceptor	Distance	Donor	Acceptor	Distance
A9-N	NAP-NO7	2.9	A9-N	NDP-NO7	3.0
K54-N	NAP-AO4*	3.0	K54-N	NDP-AO4*	3.0
K54-NZ	NAP-AOP2	2.8	K54-NZ	NDP-AOP2	2.5
K55-N	NAP-AO5*	3.1	K55-N	NDP-AO5*	3.2
T56-N	NAP-AO2	2.9	T56-N	NDP-AO2	3.0
T56-OG1	NAP-AO2	2.7	T56-OG1	NDP-AO2	2.6
S76-OG	NAP-AOP2	2.6	S76-OG	NDP-AOP2	2.5
R77-N	NAP-AOP1	2.7	R77-N	NDP-AOP1	2.8
G117-N	NAP-AO1	3.2	G117-N	NDP-AO1	3.1
			G117-N	NDP-AO2	3.1
S118-N	NAP-NO2	3.0	S118-N	NDP-NO5*	2.9
S118-OG	NAP-NO2	3.3			
			S119-OG	NDP-AO1	2.8
			S119-N	NDP-NO2	2.8
			S119-OG	NDP-NO2	3.1
			NDP-NN7	A9-O	2.8
NAP-AN1	R91-O	3.4			
NAP-NN7	A9-O	2.8			
NAP-NN7	I16-O	3.0	NDP-NN7	I16-O	3.2
NAP-AN7	S119-OG	3.2			
N64-ND2	FOL-O	2.9			
R70-NH1	FOL-O1	2.9			
R70-NH2	FOL-O2	2.8			
FOL-N3	E30-OE1	2.8			
FOL-NA2	E30-OE2	2.8			

**Supplementary Table 2. Table of hydrogen bonds in both hinge regions for human and *E. coli* DHFRs.** The extensive network of hydrogen bonds in the long hinge 1 of hDHFR supports the rigid body hinge-twisting motion that opens the active site.

<b>HINGE 1</b>					
<b>Human DHFR, E–NADP+–FOL</b>			<b><i>E. coli</i> DHFR, E–NADP+–FOL</b>		
<b>Donor</b>	<b>Acceptor</b>	<b>Distance</b>	<b>Donor</b>	<b>Acceptor</b>	<b>Distance</b>
T39-N	Q35-O	2.9	L36-N	K32-O	2.9
T39-OG	Q35-O	2.7	D37-N	G56-O	2.8
T40-N	R36-O	3.1	K38-N	T35-O	3.2
T40-OG1	R36-O	2.7	K38-NZ	E90-OE1	2.8
S41-OG	V43-O	2.8	K38-NZ	N34-O	2.9
S41-OG	K46-O	3.2			
S41-OG	D110-OD2	3.5			
S42-N	D110-OD2	2.8			
S42-OG	D110-OD2	2.7			
V43-N	S41-OG	3.0			
K46-N	V43-O	3.2			
Q47-N	K108-O	3.0			
N48-ND2	T38-O	2.9			
N48-ND2	T40-O	3.0			
L49-N	M111-O	2.9			
R70-NH1	T38-OG1	2.9			
I71-N	N48-O	2.9			
D110-N	Q47-O	2.8			
M111-N	N48-OD1	2.9			
W113-N	L49-O	2.8			

<b>HINGE 2</b>					
<b>Human DHFR, E–NADP+–FOL</b>			<b><i>E. coli</i> DHFR, E–NADP+–FOL</b>		
H127-N	A124-O	3.0	K106-N	F103-O	3.0
H127-ND1	P128-O	2.8			
G129-N	D186-O*	2.8	A107-N	L104-O	3.1
L131-N	K184-O	3.1	R158-NE	A107-O	2.8
K184-NZ	H127-O	2.7			
K184-NZ	G129-O	2.7	R158-NE	A107-O	3.2
K184-N	L131-O	3.0			

\*C-terminal residue



**Supplementary Table 4. Sequence conservation of Hinge 1.** The first two residues shown are the bending residues in this hinge.

hDHFR	T	T	S	S	V	E	G	K	Q	N	L
<b>% Identity</b>	31.4	38.8	18.2	43.0	21.5	24.8	45.5	85.1	32.2	100.0	14.9
<b>% Conservation</b>	<b>57.0</b>	<b>42.1</b>	<b>69.4</b>	<b>51.2</b>	<b>22.3</b>	<b>28.1</b>	<b>45.5</b>	<b>85.1</b>	<b>32.2</b>	<b>100.0</b>	<b>31.4</b>

## Supplementary note

### Expanded discussions

#### The human DHFR active site

For *E. coli* DHFR, a large chemical shift change in the  $^{15}\text{N}$  dimension is observed for Ala6 between THF complexes and FOL complexes. This difference is the result of a hydrogen bond to Ile5, which is formed when THF is bound, but not when FOL is bound<sup>1</sup>. Based on the crystal structures, a similar hydrogen bond would be expected for hDHFR involving Ile7. However, there is no evidence for its formation from our NMR data. From the near identity of the E–NADP<sup>+</sup>–FOL and E–NADP<sup>+</sup>–THF spectra, we conclude that hDHFR does not discriminate as effectively as ecDHFR with respect to FOL and THF. Consistent with this notion, the dissociation constants for FOL, DHF and THF are very similar for hDHFR, while ecDHFR binds two orders of magnitude more tightly to THF than it does to FOL<sup>4-7</sup>. The  $^{15}\text{N}$  HSCQ spectrum of hE–NADPH–THF shows significant broadening and some shifting of resonances compared with that of the hE–NADP<sup>+</sup>–THF complex. However, we were unable to prepare a stable sample for this complex, and the  $^{15}\text{N}$  HSQC spectrum began changing within a few hours. Therefore, reliable assignments could not be made, and we could not study this complex in detail. A chemical shift analysis of hE–THF and hE–NADP<sup>+</sup>–THF shows that, in the product binary complex, the differences in chemical shifts can be attributed to the presence or absence of NADP, without additional changes in backbone conformation. Thus, X-ray structures and  $^{15}\text{N}$  HSQCs show that the backbone conformation of hE–NADP<sup>+</sup>–FOL, hE–NADP<sup>+</sup>–THF and hE–THF are all very similar and in the “closed” conformation. The “closed” conformation in ecDHFR is stabilized by hydrogen bonds between the backbone amide and sidechain carboxylate of Asp122 and the backbone carbonyl and amide of Gly15 and Glu17, respectively. In the



“occluded” conformation, these hydrogen bonds are broken, and new ones are formed between backbone carbonyl and amide of Asn23 and the backbone amide and side-chain hydroxyl of Ser148, respectively<sup>1</sup>. In hDHFR, this hydrogen-bonding pattern is conserved for the observed “closed” conformation, but the hydrogen bonds stabilizing the “occluded” conformation cannot be formed as Asn23 of ecDHFR is replaced by two prolines in hDHFR. As mentioned in the main text, the active site of hDHFR appears to be better packed than that of ecDHFR. The key side chains that contribute to the efficient active site packing in the human enzyme are Leu22, Pro26, Phe31, Ile60 and Pro61. In ecDHFR, Leu22 is replaced by the more flexible Met20, Phe31 is substituted by a smaller Leu28, and Pro61 by the highly flexible Gly51, resulting in a more loosely packed active site.

#### *Chemical shift analysis of hE–NADPH and hE–NADP<sup>+</sup>–FOL*

To assess the presence of the hinge motion in solution, we turned to NMR experiments. A comparison of the <sup>15</sup>N HSQC spectra of hE–NADPH and hE–NADP<sup>+</sup>–FOL shows chemical shift differences that are consistent with the hinge movement observed in the crystal structures. As hE–NADPH is not stable at pH 6.5, the pH at which the chemical shift analysis was carried out for other complexes, spectra of both hE–NADPH and hE–NADP<sup>+</sup>–FOL were collected at pH 8.0 to facilitate an analysis that is not influenced by pH-dependent chemical shift changes in either complex (Supplementary Fig. 3d,e). Several chemical shift changes are observed, of which only a subset reflect ligand (FOL) binding, as expected. Gly129, one of the hinge-bending residues shows a very large chemical shift difference in both <sup>1</sup>H and <sup>15</sup>N positions. Other residues in the region, Leu131 and Lys132 also show significant <sup>15</sup>N and <sup>1</sup>H chemical shift differences. These data are consistent with a conformational change in the region, and we conclude that the

difference in chemical shifts most likely reflects the hinge movement, with the hinge being closed in the hE–NADP<sup>+</sup>–FOL complex, and open or averaging between open and closed in the hE–NADPH complex. In the region of hinge 1, the backbone amide cross peak of Gly45 is broadened beyond detection, and resonances of residues 42 and 44 are weak, indicative of flexibility in that region. We also observe a chemical shift difference for Asn107. Asn107 N forms a hydrogen bond with Pro103 CO, stabilizing a short 1.5 turn helix. In the ternary hE–NADP<sup>+</sup>–FOL complex, Pro103 is slightly shifted out of register, and the distance between Asn107 N and Pro103 CO increases from 3.1 Å in hE–NADPH to 4.5 Å. The hydrogen bond between Asn107 N and Pro103 CO is, therefore, broken, and the secondary structure in this region is loosened in the ternary (hinge-closed) complex.

### *Hinge movements in hDHFR*

A comparison of the hydrogen bonding patterns in the hE–NADP<sup>+</sup>–FOL and hE–NADPH structures sheds considerable light on how these movements are driven by ligand binding and release in human DHFR. The NADP cofactor in both hE–NADPH and E–NADP<sup>+</sup>–FOL is firmly anchored to the loop subdomain in the region of the nicotinamide ring, and to the adenosine binding subdomain in the region of the adenosine moiety. Thus, the hydrogen-bonding network to the protein is maintained at both ends of NADP. However, in the pyrophosphate region of NADP, the interactions with the  $\alpha$ F helix differ between the binary hE–NADPH and ternary hE–NADP<sup>+</sup>–FOL structures. The phosphate groups form hydrogen bonds to the hydroxyl group and backbone amide of Ser119 in hE–NADPH, and an additional hydrogen bond to the backbone amide of Gly117 (Supplementary Fig. 2a-c). Upon folate binding, several new hydrogen bonds are formed from FOL to both subdomains of the protein (Supplementary Table 1), pulling both

subdomains towards each other. In the hinge-closed state, the hydrogen bonds between NADPH and Ser119 are broken, allowing helix  $\alpha$ F to slide 2.5 Å away from the active site as the rest of the adenosine binding subdomain closes in towards the loop subdomain. The sliding of helix  $\alpha$ F introduces a twisting motion into the hinge movement, and allows sufficient space for the nicotinamide ring of NADP<sup>+</sup> to be rearranged slightly to avoid steric clash with the pterin ring of folate. In the absence of substrate, the NADP to Ser119 hydrogen bonds stabilize the hinge-open conformation, explaining why this conformation is not observed when a ligand is bound in the substrate-binding site. The hinge motions are, therefore, driven by ligand binding, and the two conformations are stabilized by hydrogen bonding interactions and hydrophobic packing interactions between the ligands and the enzyme.

Thr40, a classical helix C-cap and one of the bending residues in hinge 1, forms a hydrogen bond to the backbone CO of Arg36 in the substrate-binding helix, and also to the Asn48 side chain at the end of the hinge. Additionally, Asn48 forms a hydrogen bond to the backbone amide of Met111 in the adenosine-binding subdomain, and to Thr38, the last residue in the substrate binding helix preceding hinge 1. The bending of Thr39 and Thr40 results in a rigid body movement of a subset of residues in hinge 1 and the adenosine binding subdomain (Thr41-I114) moves as a rigid body; the length of this hinge provides the framework for the rigid body movement. The hinge 1 region in ecDHFR is 7 residues shorter than that of hDHFR, and forms a network of hydrogen bonds to both subdomains, restricting the extent of possible movements in this region; accordingly, hinge-bending is of much smaller magnitude in ecDHFR<sup>1</sup> than in the human enzyme (Supplementary Fig. 2a-c).

A comparison of the hE–NADPH complex with mouse DHFR (mDHFR, mE) in complex with NADPH shows that the hinge-open conformation is only observed in the hE–NADPH

structure, not in the mE–NADPH structure, although the sequences are highly conserved. The two structures are in different space groups, and both have lattice contacts in areas that could influence the stabilization of the hinge-open versus hinge-closed conformation in the crystal structures. Most importantly, the mE–NADPH structure (PDB code: 3D84<sup>8</sup>) has a glycerol molecule bound in the substrate-binding site, forming key hydrogen bonds to the substrate binding helix, adenosine binding domain and core  $\beta$ -sheet, which would be expected to stabilize the hinge-closed conformation in a similar manner as FOL.

#### Further discussion of PWNAL ecDHFR mutant

The <sup>15</sup>N HSQC spectrum of the <sup>21</sup>PWNAL<sup>24</sup> E–NADP<sup>+</sup>–FOL is very similar to that of the wild type enzyme, and even more so to the N23PP/S148A mutant, indicating that it is structurally similar (Supplementary Fig. 4a). Due to the very small amount of dispersion, which is detectable in <sup>15</sup>N R<sub>2</sub> dispersion experiments only at the higher field, the data cannot be fit to obtain an accurate rate, but indicate the presence of limited flexibility in these residues on the  $\mu$ s timescale, at a much faster rate (estimated to be  $\sim 3000$  s<sup>-1</sup>) than for the wild type enzyme. Motions are altered in key loop residues, such as Gly121 and His149, which show large fluctuations in wild type E–NADP<sup>+</sup>–FOL, but no observable <sup>15</sup>N R<sub>2</sub> dispersion in the mutant (Supplementary Fig. 4b,c). C-terminal-associated residues maintain millisecond timescale dynamics similar to wild type and <sup>21</sup>PWPPL<sup>24</sup> ecDHFR, with a rate ( $k_{\text{ex}}$ ) of  $600 (\pm 16)$  s<sup>-1</sup>, and an excited state population of 3.2%.

### Relationship between Regions A, B & C in DHFR

The length of Region 1 relates to conformational flexibility of the active site “Met20” loop, and the length and composition of Regions 2 and 3 are likely determinants of whether hinge movements can occur in the enzyme. Based on our sequence analysis, we find that the combination of lengths in these three regions show certain preferences. The vast majority of bacterial sequences contain 7 residues in Region A, 12 residues in region B, and 14 residues in Region C, and thus have flexible Met20 loops and short hinges that appear unable to support the large scale opening of the active site observed in hDHFR. All Region B sequences containing 19 residues exactly can be aligned accurately to the hDHFR sequence and structure, on the assumption that the flanking secondary structures ( $\alpha$ B and  $\beta$ B) are conserved in length. Longer hinges are present in most eukaryotes, but lower eukaryotes retain flexible Met20 loops (short Region A), while higher eukaryotes contain an insertion in Region A, limiting the conformational change after hydride transfer. It seems likely that, while almost all prokaryotic DHFRs cannot accommodate the hinge movements, most eukaryotic DHFRs have already developed the length of hinge that would be required for the hinge movements, but only a few eukaryotic DHFRs have eliminated conformational flexibility influenced by Region A. In a minor group of bacterial sequences, the length of Region C (and therefore likely hinge 2) is similar to hDHFR, but the length of Region B (and likely hinge 1) is identical to the majority of bacterial sequences.

A comprehensive analysis of all DHFR structures in the PDB was carried out, paying special attention to loop and hinge conformations in Regions A, B and C. Although several structures of DHFR are available, analysis of these is not as insightful as one would expect for two main reasons: A) Most structures are of either the *E. coli* or human enzyme bound to an inhibitor and NADP<sup>+</sup> in a ternary complex. In the ternary complex, the active site loops are

preferentially closed, and do not give much insight into the conformations relevant to catalysis.

B) An analysis of all structures shows most to be exactly the same as the "closed" conformation of ecDHFR. Very few structures differ significantly from this conformation. For the structures that shed insights on understanding the dynamic mechanism, we have included our observations below or in the main text.

It is interesting to note that, in a small subset of bacterial sequences, the length of Region B is increased by one residue compared with the consensus length for bacterial DHFRs. This subset represents thermophilic bacteria including *Thermatoga maritima* DHFR (tmDHFR), as well as a few enterobacteria. Since structures are available for tmDHFR, we can assess the differences between tmDHFR and ecDHFR further. tmDHFR is a dimer, in which the active site loop ("Met20 loop" assessed in region 1) forms part of the dimer interface, and is stabilized in an "open" conformation, which is different from the "closed" and "occluded" conformations of ecDHFR. The "open" conformation has been observed in some crystal structures of ecDHFR, wherein it is stabilized by lattice contacts, but is not a stable ground state in any intermediate complex for ecDHFR. While this conformation is conducive to NADP binding, it is not optimal for catalysis, as the "open" loop does not shield the active site from bulk solvent<sup>1</sup>. The additional residue in Region B of tmDHFR forms an extra turn in the substrate binding helix, and does not add to the length of the connecting loop. However, we note that the dynamic mechanism in tmDHFR is likely to be quite different from that of ecDHFR due to the dimerization interface of the enzyme at the active site, and the fact that the enzyme functions at much higher temperatures.

*Gallus gallus* (chicken) DHFR (cDHFR) is the vertebrate DHFR that is most divergent from hDHFR and for which a structure is available (PDB codes: 1DR1, ternary complex with thioNADP<sup>+</sup> and biopterin and 8DFR, binary complex with thioNADP<sup>+</sup>)<sup>9,10</sup>. A comparison of both

cDHFR structures with hE-NADP<sup>+</sup>-FOL shows that the  $\alpha$ F helix superimposes exactly with hDHFR in the hinge-closed conformation. When the structures are aligned on the loop subdomain, only Gly53 and K68 in the cDHFR adenosine binding domain are in a slightly more “open” conformation than hE-NADP<sup>+</sup>-FOL. In the presence of substrate or product, this region would be expected to form hydrogen bonds to the ligand, and close the active site. It is likely that helix  $\alpha$ F cannot stabilize the hinge-open conformation, as Ser119 of hDHFR is substituted with Ala119 in cDHFR, and the hydrogen bonds between this residue at the N-terminus of helix  $\alpha$ F forms stabilizing hydrogen bonds with NADPH in the binary hE-NADPH hinge-open conformation. There is no notable difference in the conformation of the binary cE-thioNADP<sup>+</sup> and ternary cE-thioNADP<sup>+</sup>:biopterin, showing that the hinge-open conformation is not present, and providing further evidence that the interaction of the Ser119 residue in  $\alpha$ F with NADP is important in maintaining the hinge-open conformation in hDHFR.

## References

1. Sawaya, M.R. & Kraut, J. Loop and subdomain movements in the mechanism of *Escherichia coli* dihydrofolate reductase: crystallographic evidence. *Biochemistry* **36**, 586-603 (1997).
2. Whitlow, M. *et al.* X-ray crystallographic studies of *Candida albicans* dihydrofolate reductase. *J. Biol. Chem.* **272**, 30289-30298 (1997).
3. Bhabha, G. *et al.* A dynamic knockout reveals that conformational fluctuations influence the chemical step of enzyme catalysis. *Science* **332**, 234-238 (2011).
4. Fierke, C.A., Johnson, K.A., & Benkovic, S.J. Construction and evaluation of the kinetic scheme associated with dihydrofolate reductase from *Escherichia coli*. *Biochemistry* **26**, 4085-4092 (1987).
5. Appleman, J.R. *et al.* Atypical transient state kinetics of recombinant human dihydrofolate reductase produced by hysteretic behavior. Comparison with dihydrofolate reductases from other sources. *J. Biol. Chem.* **264**, 2625-2633 (1989).
6. Lewis, W.S. *et al.* Methotrexate-resistant variants of human dihydrofolate reductase with substitutions of leucine 22. Kinetics, crystallography, and potential as selectable markers. *J. Biol. Chem.* **270**, 5057-5064 (1995).
7. Tsay, J.-T. *et al.* Kinetic investigation of the functional role of phenylalanine-31 of recombinant human dihydrofolate reductase. *Biochemistry* **29**, 6428-6436 (1990).
8. Cody, V., Pace, J., & Rosowsky, A. Structural analysis of a holoenzyme complex of mouse dihydrofolate reductase with NADPH and a ternary complex with the potent and selective inhibitor 2,4-diamino-6-(2'-hydroxydibenz[b,f]azepin-5-yl)methylpteridine. *Acta Crystallogr. D. Biol. Crystallogr.* **64**, 977-984 (2008).
9. McTigue, M.A., Davies, J.F.I., & Kraut, J. Crystal structure of chicken liver dihydrofolate reductase complexed with NADP<sup>+</sup> and biopterin. *Biochemistry* **31**, 7264-7273 (1992).
10. McTigue, M.A., Davies, J.F., Kaufman, B.T., & Kraut, J. Crystal structures of chicken liver dihydrofolate reductase: binary thioNADP<sup>+</sup> and ternary thioNADP<sup>+</sup>.biopterin complexes. *Biochemistry* **32**, 6855-6862 (1993).